ADVANCED QUANTUM TECHNOLOGIES
www.advquantumtech.com

Nuclear Physics in the Era of Quantum Computing and Quantum Machine Learning

José-Enrique García-Ramos, Álvaro Sáiz, José M. Arias, Lucas Lamata, and Pedro Pérez-Fernández*

In this paper, the application of quantum simulations and quantum machine learning is explored to solve problems in low-energy nuclear physics. The use of quantum computing to address nuclear physics problems is still in its infancy, and particularly, the application of quantum machine learning (QML) in the realm of low-energy nuclear physics is almost nonexistent. Three specific examples are presented where the utilization of quantum computing and QML provides, or can potentially provide in the future, a computational advantage: i) determining the phase/shape in schematic nuclear models, ii) calculating the ground state energy of a nuclear shell model-type Hamiltonian, and iii) identifying particles or determining trajectories in nuclear physics experiments.

1. Introduction

In this perspective review, we discuss the link between low-energy nuclear physics and the emerging research field of quantum computing,[1] which includes quantum simulations and quantum machine learning (QML) techniques. While both research fields have their own distinct problems and applications, they can be combined in a fruitful collaboration to yield new and relevant advancements. Although quantum simulations in nuclear physics have made progress in recent years, they have mainly focused on toy models or simple scenarios. However, the utilization of QML techniques in low-energy nuclear physics is very limited. The objective of this perspective is to showcase the value of studying the fields of nuclear physics and quantum computing. We provide examples and highlight the significant potential for researchers in both domains. Indeed, several long-term plans and white papers have already considered and promoted these new research avenues such as refs. [2] and [3] (US Department of Energy), the white paper[4,5] (US Department of Energy, National Science Foundation, and National Institute of Standards and Technology) or the NuPECC Long Range Plan 2024 (still under discussion).

The structure of this work is as follows: in Section 2, we present the fundamentals of nuclear physics and its potential connections with quantum computing and QML. Next, in Section 3, we provide a brief overview of quantum simulations and QML. In Section 4, we discuss the current connections between quantum simulations, QML, and nuclear physics, illustrating this through a few examples such as: i) determining the shape/phase of a nucleus using the time evolution of an appropriated observable, ii) calculating the ground state energy of nuclei, and iii) identifying particles and reconstructing particle trajectories. Finally, in Section 5, we present our conclusions and provide an outlook for future research.

2. The Nuclear Physics Realm

In this section, we provide a concise overview of three key aspects: first, the most commonly employed nuclear physics models designed for low-energy nuclear physics; second, the primary research directions in nuclear physics within the realm of quantum computing; and third, the latest applications of machine learning (ML) in addressing nuclear physics problems.

2.1. Nuclear Models

The study of the atomic nucleus is difficult since it is a quantum many-body system where two types of nucleons, protons and

J.-E. García-Ramos
Departamento de Ciencias Integradas y Centro de Estudios Avanzados en Física, Matemática y Computación
Universidad de Huelva
21071 Huelva, Spain
E-mail: enrique.ramos@dfaie.uhu.es

J.-E. García-Ramos
Instituto Carlos I de Física Teórica y Computacional
Universidad de Granada
Fuentenueva s/n, 18071 Granada, Spain

Á. Sáiz, P. Pérez-Fernández
Departamento de Física Aplicada III
Escuela Técnica Superior de Ingeniería, Universidad de Sevilla
E-41092 Sevilla, Spain

J. M. Arias, L. Lamata
Departamento de Física Atómica, Molecular y Nuclear, Facultad de Física
Universidad de Sevilla
Apartado 1065, E-41080 Sevilla, Spain

The ORCID identification number(s) for the author(s) of this article can be found under https://doi.org/10.1002/qute.202300219

DOI: 10.1002/qute.202300219

neutrons, interact via a force that cannot be expressed in a closed form starting from first principles[6] and, as a matter of fact, it is intractable in the non-perturbative regime of the QCD. In addition, the number of particles is not large enough for the use of the powerful statistical mechanic machinery,[6] therefore, it is necessary to explicitly consider a large number of degrees of freedom. Because of that, to understand the nuclear structure, one has to rely on nuclear models, which can only partially describe the nuclear degrees of freedom. The situation is radically different from the studies in quantum chemistry, where the interaction is of Coulomb nature and therefore fully known. However, a large number of particles should still be considered. In the atomic nucleus, a natural center for the potential does not exist, as it is the case of the atom, and the field that the nucleons feel is created by the own nucleons. Therefore, it is not obvious whether a mean field could be defined.[6] The theoretical description of the nuclear structure at low energy is based on three main approaches: i) the microscopic approach whose basic realization is the shell model[6,7] ii) the mean-field approach,[7,8] and iii) the macroscopic approach based on the liquid drop model.[7,9,10] These are briefly described below.

a) The nuclear shell model provides a description of the behavior of nucleons (protons and neutrons) in an atomic nucleus based on the independent particle motion of nucleons, being possible to define single particle orbits and, therefore, single particle levels, that occupy the nucleons within the nucleus, in a similar manner to electrons in an atom, i.e., in the atomic shell model. The model assumes that nucleons move in a mean field created by the whole set of nucleons. Once the nucleons are distributed in shells, the residual interaction between them is taken into account and the full diagonalization of the Hamiltonian is required.[11] The shell model successfully explains many nuclear properties, such as nuclear stability, magic numbers (nuclei with particularly stable configurations), nuclear spectra, and nuclear reactions.
b) The mean field, the beyond mean-field approximation and the use of energy functional theories[7,8,12,13] rely on the assumption that nucleons move independently in an effective average potential generated by all other nucleons. The interaction can be obtained globally in a self-consistent way for the whole mass table, fixing a set of free coefficients to reproduce ground state properties of all known nuclei. This simplification allows for the treatment of complex many-body systems by reducing the problem to an effective single-particle problem. Theoretical foundations of mean-field models include: i) the Hartree-Fock or Hartree-Fock-Bogoliubov formalism, ii) density functional theory (DFT), and iii) mean-field potentials and self-consistency. Applications of mean-field models in nuclear structure include the calculations of nuclear binding energies and masses, nuclear deformation, and shape transitions, shell structure and magic numbers, and collective motion and excitations, among others.
c) The collective model, also known as the liquid drop model, treats the nucleus as a droplet of incompressible nuclear matter. This model assumes that the nucleus behaves as a classical liquid drop, with nucleons interacting through attractive and repulsive forces. It explains nuclear phenomena by considering collective motion, such as rotation and vibration, of the nuclear surface. The model successfully describes phenomena such as nuclear deformation, fission, and certain aspects of nuclear spectra. Along the same lines, the Kumar-Baranger model,[14–16] or the generalized collective model, is an extension of the collective Bohr model.[9] It takes into account the coupling between collective motion and single-particle excitations within the nucleus. This model considers both vibrational and rotational degrees of freedom and is especially useful for describing transitional nuclei that exhibit characteristics of both vibrational and rotational motion.

These models and their extensions have contributed significantly to our understanding of nuclear structure. The difficulty in solving the nuclear physics problem, apart from the related one with the interaction, is the dimension of the Hilbert space that for medium-mass and heavy nuclei around the center of a major shell, either in protons, neutrons or both, is far beyond the present and even future computational capabilities using a direct diagonalization of the system Hamiltonian. However, alternative techniques have been developed in the past decades such as the Shell Model Monte Carlo method[17] or the Monte Carlo Shell Model,[18] which introduced the Quantum Monte Carlo Diagonalization method. As a matter of fact, in the shell model, an explosion of the dimension of the Hilbert space appears when a large number of nucleons are distributed in large major shells. Moreover, in order to explain certain phenomena, multi-particle-hole excitations across two major shells, which generates a further explosion of the Hilbert space dimension, are needed to be included. In the case of the energy functional approach, the main problem is related to the generation of states with defined quantum numbers, i.e., to go beyond the mean field using, for instance, the generator coordinate method,[7] which involves the evaluation of integrals, which again can be computationally expensive. The use of quantum computing and, in particular, quantum machine learning can open a new avenue to deal with these nuclear problems in the near future.

Nowadays, the implementation of state-of-the-art nuclear shell model or beyond mean-field problems in Noisy-Intermediate Scale Quantum (NISQ) computers is not yet possible, because of the reduced number of available qubits, but also due to the accumulated gate errors, which promote the design of new algorithms to work with these devices. Some simpler models that retain the main characteristics of the aforementioned ones have been recently used: i) the Lipkin-Meshkov-Glick (LMG) model[19] that resembles the quadrupole-quadrupole nuclear interaction, but it is of great interest in condensed matter and also describes, in an approximate way, certain solid state systems and ii) the Agassi model[20] that mimics the interplay between pairing and quadrupole interactions as in the Kumar-Baranger model, or iii) the family of exactly solvable models known as Richardson-Gaudin models.[21,22]

2.2. Nuclear Physics and Quantum Computing

Nuclear physics is a discipline that faces problems that are highly demanding computationally where quantum computing can open a new avenue to deal with them. Here, we mention some potential applications where quantum computing is or can be employed in the nuclear physics realm:

a) Quantum simulations: quantum computers could have the potential to simulate quantum systems more efficiently than classical computers.[23] This includes simulating the behavior of atomic nuclei and nuclear interactions. The quantum simulation of a nuclear system could allow us to gain deeper insights into nuclear physics phenomena.[24,25]
b) Quantum algorithms for nuclear physics: quantum algorithms, such as the Variational Quantum Eigensolver (VQE)[26,27] and Quantum Phase Estimation (QPE),[1] have been developed to solve problems in quantum chemistry, where the quantum many-body problem is exponentially difficult to be treated on classical computers. Nuclear physics also faces the same difficulty in solving its quantum many-body problem. These algorithms can be applied to nuclear physics problems, such as calculating nuclear energy levels or simulating nuclear reactions.
c) Data analysis and optimization: nuclear physics experiments generate vast amounts of data that need to be analyzed and optimized. Quantum computing techniques, such as QML algorithms or quantum optimization algorithms, may offer novel approaches to simulate and extract valuable insights from nuclear physics data.[28,29]

While the full extent of the connection between nuclear physics and quantum computing is still being explored, it is already a potential area of collaboration and research. The development of more powerful and scalable quantum computers may provide new tools and techniques to address complex nuclear physics problems.

2.3. Nuclear Physics and Machine Learning

In the last few years, ML has been applied to nuclear physics in different tasks[30]:

a) Data analysis: nuclear physics generates large amounts of experimental data. ML can help to process and analyze this data efficiently to extract patterns, identify particles, perform classifications, and make predictions. ML algorithms such as neural networks can uncover hidden correlations and trends in nuclear data.
b) Nuclear modeling: ML can also be used to develop models and simulations in nuclear physics. Traditional nuclear physics models often involve complex calculations and approximations. ML offers alternative approaches to nuclear modeling, where ML algorithms can be used to construct empirical models from nuclear data and improve prediction accuracy.
c) Particle detection and identification: in nuclear physics experiments, it is crucial to identify and track charged particles. ML has been successfully applied to particle detection and trajectory reconstruction, which can enhance the precision and efficiency of data analysis. The recognition of patterns in large dataset is of key importance and ML generative models can enormously simplify this task.[31] Algorithms such as pattern classifiers, convolutional neural networks (CNN), and particle tracking algorithms can also aid in particle identification and reconstruction in nuclear detectors. An interesting application of ML to particle detection is the improvement in track seeding resulting from the use of artificial neural networks (ANNs) and deep learning methods that produces a substantially faster track reconstruction speed.[32,33] The combination of ANNs, CNNs, and Variational Autoencoders (VAEs) improves particle recognition in Cherenkov detectors,[34] while ANNs contribute to the detection of photons produced in the decays of hadrons in calorimeters.[35]
d) Experimental optimization: ML can assist in the optimization of nuclear physics experiments. Optimization algorithms such as genetic algorithms or reinforcement learning can help finding optimal configurations of experimental parameters, thereby saving time and resources in data collection.

These are just a few areas where ML has been successfully applied in nuclear physics. The intersection of both disciplines offers exciting opportunities to improve data analysis, develop more accurate models, and optimize experiments. As ML continues to evolve, its application in nuclear physics is likely to expand further.

3. Quantum Simulations and Quantum Machine Learning

Quantum simulations[23] is a rapidly growing area of research in which a quantum controllable system is employed to reproduce the properties (either dynamical or static) of another quantum system of interest. Over the past two decades, numerous proposals, and experiments have emerged in this field, employing various quantum simulator platforms such as trapped ions, superconducting circuits, cold atoms, quantum photons, and nuclear magnetic resonance. The simulated quantum systems are diverse and could be roughly grouped into condensed matter, quantum chemistry, and high-energy physics, although this is not an exhaustive list. Within the realm of quantum simulations, a nascent field has emerged in recent years at the intersection of many-body quantum systems and high-energy physics.[36]

Quantum hardware belongs mainly to one of three possible categories: digital quantum simulators, analog quantum simulators, and digital-analog quantum simulators.[37] Digital quantum simulators allow to deal with a wide variety of systems, as they have universality properties: they decompose the simulated quantum dynamics into elementary unitary gates, that later on are implemented in the quantum simulator step by step. The most usual way to do this is using the Lie-Trotter-Suzuki expansion[1] and, in particular, its first-order approach, but it is also possible to include higher-order terms. Another option is to use the Quantum Signal Processing (QSP)[38] which is equivalent to the second-order Lie-Trotter-Suzuki expansion but using fewer resources. Finally, it is worth mentioning the Linear Combination of Unitaries (LCU), which is designed to implement operators either unitary or not.[39] The main drawback of digital quantum simulators is that it is difficult to go beyond a few dozen qubits with current technology, due to the accumulated fidelity gate errors that are much larger for the two-qubit gates than for the one-qubit ones. Moreover, the approximations used to express the Hamiltonian in terms of single- and two-qubit gates induce additional errors, called "Trotter errors" in short, that can be always reduced going to higher order approximations, but at the

cost of using a larger number of quantum gates, thereby greatly increasing the fidelity error.

Analog quantum simulators implement, in the quantum platform, quantum dynamics following a Hamiltonian that is similar to the one of the simulated quantum system, by tuning some control parameters such as laser pulses, microwaves, etc. The advantage of analog quantum simulators is that they are more scalable than the purely digital ones as they incur less accumulated gate and digital errors.

Finally, digital-analog quantum simulators aim at benefiting from both paradigms, digital and analog, via combining large analog blocks (which provide scalability) with digital steps (which enable to simulate a wider variety of models than the purely analog). This paradigm could be a way to achieve useful new knowledge in NISQ computers in the near and mid term.[37]

The typical errors in a quantum simulator are the following ones: accumulated gate error and digital error, as well as the ones common to all quantum systems, such as decoherence due to an uncontrollable coupling to the environment. Therefore, sometimes it is advisable to employ a master equation to theoretically model a quantum simulation platform, as well as to interpret the experimental results.[23]

QML[28,29] aims to connect the two fields of ML (in turn belonging to the more general field of artificial intelligence) and quantum computing. The goal is either to employ quantum devices to carry out more efficient ML calculations, or to use ML algorithms to better control and analyze quantum systems. Today, still in only a few examples, QML has proven a clear advantage over ML using classical data. In ref. [40], the authors have studied the conditions ("checklist") that a learning problem should satisfy to have a provable quantum speedup. Quantum systems produce counter-intuitive patterns that are expected not to be easily generated by classical systems, hence, it is reasonable to postulate that quantum computers may outperform the classical ones on ML tasks.[29] Thus, it is sensible to aim at using quantum devices to carry out some of the ML tasks that suffer from the so-called dimensionality curse, far more efficiently. Namely, with less time and energy resources expense.[28,29]

The field of QML has grown significantly in the past five years, and several theoretical proposals, as well as experimental realizations have been produced on platforms such as superconducting circuits, quantum photonics, and trapped ions.[41,42] QML models inspired by biology, i.e., quantum biomimetics, have been proposed.[43] However, the use of QML protocols for the analysis of nuclear physics is a relatively unexplored field so far, although certain examples of use already exist.[44] Some of the quantum algorithms being employed in QML are quantum versions of standard ML ones, such as quantum supervised learning, quantum unsupervised learning, and quantum reinforcement learning. QML algorithms may be divided into ideal protocols for scalable quantum computers, such as the Harrow-Hassidim-Lloyd (HHL),[29] and near term algorithms, e.g., the variational quantum eigensolver (VQE).[45] In the latter case, some promising outcomes have been produced, which could perhaps enable new knowledge of quantum systems in the near term. However, there are also difficulties, such as barren plateaus, in which the optimization protocol may end up stuck in a local minimum, and not improve further. This problem seems to grow with system size, and further ways of avoiding these issues should be developed. The expressivity of variational quantum protocols also plays a crucial role, in the sense that a simple *ansatz* can not be enough to capture the model features, but a too complicated *ansatz* may be too hard and costly to train. Much of the field relies on heuristics, as well as trial and error, hence, it is hard to guarantee that a certain protocol will always work.[45] Furthermore, in recent years, efforts in the field have also focused on studying whether noise in quantum machine learning protocols is not only not detrimental in many situations, but indeed more useful than a purely ideal system, at least in certain cases.[46]

4. Quantum Simulations and Quantum Machine Learning for Low Energy Nuclear Physics

Having introduced in preceding sections some key aspects of nuclear models, quantum computing, ML and QML, we will explore below three relevant examples.

4.1. Determination of the Shape of a Nuclear System through its Time Evolution

Quantum Phase Transitions (QPTs) appear in quantum systems at zero temperature when a sudden change in the ground-state structure occurs under a change of a control parameter in the Hamiltonian,[47] thus changing the shape of the system. A typical situation in which a QPT is present corresponds to Hamiltonians that can be written as two pieces with different symmetries (A and B):

$$\hat{H} = (1 - x)\hat{H}_A + x\hat{H}_B \tag{1}$$

This formulation allows us to investigate the interplay between the two symmetries, A and B, by adjusting the control parameter x, which determines the relative contribution of each symmetry to the overall Hamiltonian. Under the formulation (1) two well defined situations exist: A for $x = 0$, and B for $x = 1$. They correspond, in the majority of cases, to dynamical symmetries.[48] However, for x −values not equal to 0 and 1, the Hamiltonian has no definite symmetry, and A and B compete among themselves. In spite of this lack of symmetry, interestingly enough, the system remains having a structure close to A or B until the critical point, $x = x_c$, at which a sudden change in the system structure appears (QPT). The existence of a QPT also implies a sudden change in the so-called order parameter, which vanishes in one of the phases (symmetric) and takes a nonzero value in the other phase (broken or non-symmetric phase).[47] QPTs can be classified accordingly to the Ehrenfest classification[49] in a similar manner to the phase transitions that occur in macroscopic systems at nonzero temperature.

In nuclear models, the shape/phase of the system is determined through mean-field calculations, although it can also be explored using certain observables that can serve as proxies for QPTs even in finite-size systems.[50] Is it possible to extract information about the phase/shape of the system using a different approach? To answer this question in refs. [51, 52] the phase diagram[53,54] of the Agassi model[20] has been determined exploring the time evolution of a correlation operator using a quantum simulator that generates instances to train a ML algorithm,

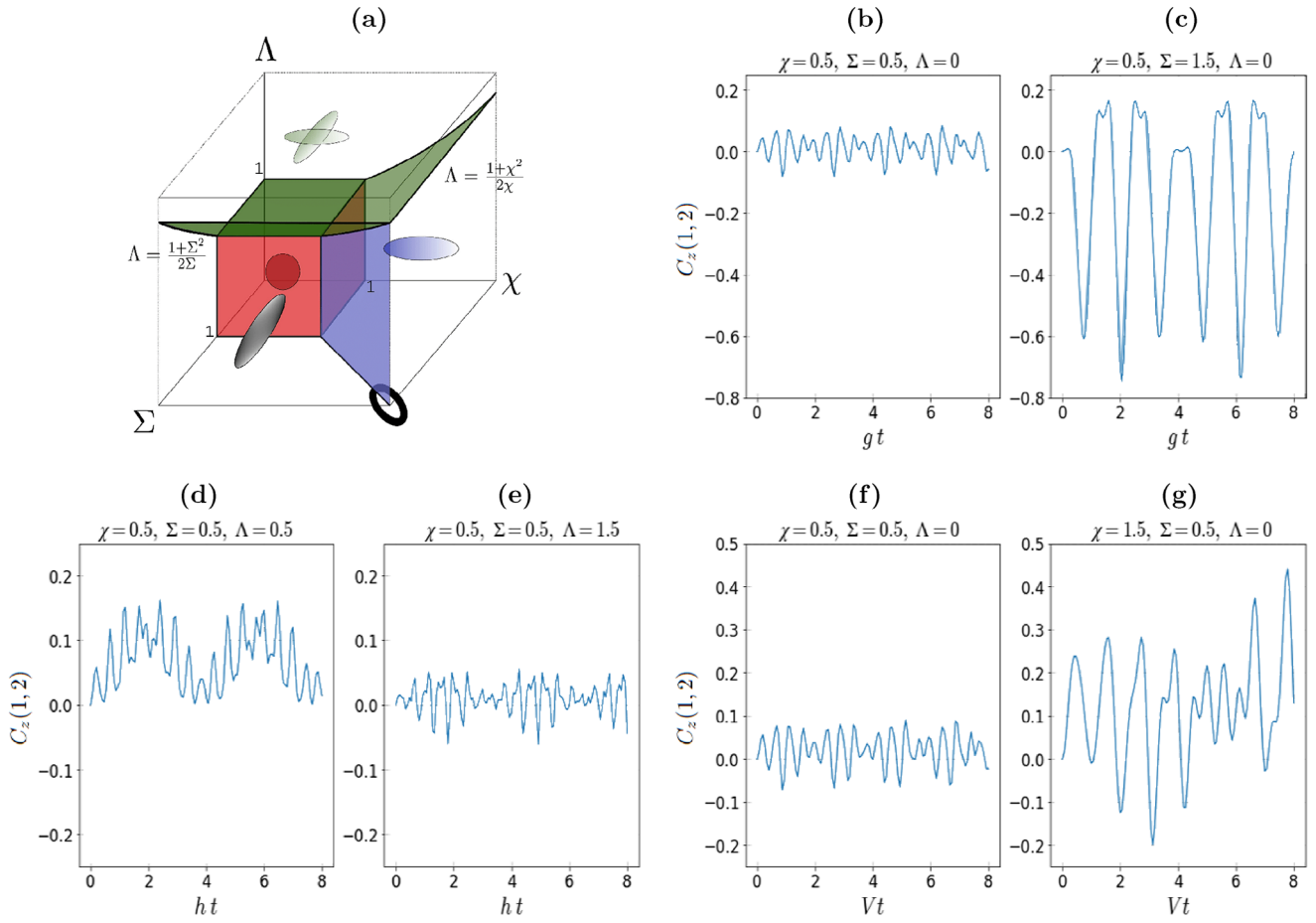

Figure 1. Panel (a) Phase diagram of the extended Agassi Hamiltonian. For convenience, the rescaled parameters χ, Σ, and Λ are used ($V = \frac{\varepsilon\chi}{2j-1}$, $g = \frac{\varepsilon\Sigma}{2j-1}$, and $h = \frac{\varepsilon\Lambda}{2j-1}$ where $2j$ corresponds to the shell size). The red vertical planes represent second-order QPT surfaces. The green surface and the blue vertical one correspond to first-order critical surfaces. The symbols represent the different possible phases of the system (see ref. [53]). Panels (b–g) correspond to the exact time evolution of $C_z(1, 2)$ for selected values of the control parameters. Reproduced with permission.[51] Copyright 2022, American Physical Society.

i.e., defining a hybrid quantum-classical algorithm. The Agassi model considers a two-level system with m −sites in each level. For the fermion operators, two indexes are used: ξ for the level (+1 for the upper and −1 for the lower one) and m for the site within each level. The Agassi Hamiltonian is interesting because it includes the competition between the monopole–monopole and the pairing interactions and mimics the Kumar-Baranger model for nuclear structure. The Hamiltonian for the extended Agassi model used in ref. [53] can be written as

$$H = \varepsilon J^0 - g \sum_{\xi,\xi'=-1,1} A^\dagger_\xi A_{\xi'} - \frac{V}{2}[(J^+)^2 + (J^-)^2] - 2hA^\dagger_0 A_0 \tag{2}$$

where the operators in the Hamiltonian are all defined in terms of fermion creation and annihilation operators, $c^\dagger_{\xi,m}$ and $c_{\xi,m}$,

$$J^+ = \sum_{m=-j}^{j} c^\dagger_{1,m} c_{-1,m} = (J^-)^\dagger \tag{3}$$

$$J^0 = \frac{1}{2} \sum_{m=-j}^{j} \left(c^\dagger_{1,m} c_{1,m} - c^\dagger_{-1,m} c_{-1,m}\right) \tag{4}$$

$$A^\dagger_1 = \sum_{m=1}^{j} c^\dagger_{1,m} c^\dagger_{1,-m} = (A_1)^\dagger \tag{5}$$

$$A^\dagger_{-1} = \sum_{m=1}^{j} c^\dagger_{-1,m} c^\dagger_{-1,-m} = (A_{-1})^\dagger \tag{6}$$

$$A^\dagger_0 = \sum_{m=1}^{j} \left(c^\dagger_{-1,m} c^\dagger_{1,-m} - c^\dagger_{-1,-m} c^\dagger_{1,m}\right) = (A_0)^\dagger \tag{7}$$

The phase diagram for the extended Agassi model is depicted in **Figure** 1a where the phase transition surfaces are clearly marked together with a pictorial representation of the phases. There, the gray oval corresponds to the BCS phase, the blue one to the HF phase, the green crossed one to the HF-BCS phase, the red sphere to the Symmetric phase and the open oval to the

Valley phase. The phase diagram has been obtained analytically using mean-field techniques.[53]

The Hamiltonian (2) can be easily mapped onto a spin Hamiltonian using the Jordan-Wigner (JW) mapping approach,[55,56] which can later be experimentally implemented in a digital quantum simulator. So far, the simulation has been performed for a system with eight sites ($N = 8$, $j = 2$). This is a small size from the point of view of QPT analysis, taking into account that the phase of a given system is expected to be properly defined in the large N limit. However, precursors of QPTs can be observed.[57] Let us define the correlation function between two sites i, j of the system as

$$C_z(i,j) = \left\langle \sigma_i^z \otimes \sigma_j^z \right\rangle - \left\langle \sigma_i^z \right\rangle \left\langle \sigma_j^z \right\rangle \tag{8}$$

where σ_i^a are the Pauli matrices at site i for $a = x, y, z$. We will consider as an *ansatz* that the time evolution of this function with the state $|\downarrow_1 \downarrow_2 \downarrow_3 \downarrow_4 \uparrow_5 \uparrow_6 \uparrow_7 \uparrow_8\rangle$ can serve as a proxy to determine the shape of the system and eventually find the location of the phase transition surfaces. Observing such an evolution with the naked eye, one cannot provide any hint about the shape of the system (see panels (b–g) of Figure 1 where the time evolution is depicted for selected values of the Hamiltonian parameters). Therefore, the use of a ML technique can greatly help classifying the obtained time evolution in terms of the different possible shapes of the system. In particular, we will focus on the use of a CNN (in ref. [51] a Multi-Layer Perceptron is also used). To generate instances for training the CNN, a lattice in the control parameter space was created with 9261 points, reserving 10% of them for testing purposes. The classical ML training was performed using as input the exact evolution operator and also approximating it with a Trotter expansion (using a number of Trotter steps equal to six) to compute the expectation value of Equation (8) over a given time range. The global accuracy obtained for the correct determination of the phase was 98.7% for the exact evolution, while 99.2% for the Trotter one. An appealing fact is that the accuracy of the procedure is even larger when using the Trotter approximation with a small number of steps, which has clear practical advantages, because it implies the use of quantum circuits of smaller depth. A possible explanation is that the larger oscillations obtained in the approximate evolution, compared with the exact one, gives rise to exaggerated patterns that are easier to recognize, but this is an issue not fully understood.[51] In **Figure 2**, the results of the CNN analysis are presented for both the exact evolution and the Trotter one for selected values of the Hamiltonian parameters. The reason why the time evolution of a given matrix element is able to describe the phase of the system is that it is connected with the complete spectrum of the Hamiltonian, assuming that the state is not an eigenstate of it. For instance, a vibrational-like nuclear Hamiltonian will generate a vibrational spectrum, while a rotational Hamiltonian will produce a sequence $l(l+1)$. In the first case, the nucleus has a spherical shape, while it is well deformed in the second situation.

Very recently, a similar work has been published, but for the Ising model[58] (note that latter, an extended version to larger spin models was published in ref. [59]). It shows that the phase diagram in the axial next-nearest-neighbor Ising (ANNNI) model can be obtained using a quantum convolutional neural network (QCNN). The considered Hamiltonian can be written as

$$H = \sum_{i=1}^{N} \left(\sigma_i^x \sigma_{i+1}^x - \kappa \sigma_i^x \sigma_{i+2}^x + h \sigma_i^z \right) \tag{9}$$

where σ_i^a are the Pauli matrices at position i, the coefficients κ and h are taken as positive and N is an even number corresponding to the number of sites in the lattice. The phase diagram of the model is quite rich and three phases are known which are separated by two second-order phase transition lines. The phase diagram of the quantum model at temperature $T = 0$ K has been studied mainly using the renormalization group or Monte Carlo techniques. To detect the phase in this case, a QCNN was used. The function proposed to train and characterize the phase is the ground state energy of the system. In order to get this energy, a VQE is used and it serves to create instances to train the QCNN. The circuit that implements the QCNN is depicted in **Figure 3**.

In order to train the QCNN and fix the variational parameters, θ_i, the cross entropy $\mathcal{L}$ loss function between the classical labels, written as a function of the control parameters, and the predictions on the training region of the phase space was used.[58] In **Figure 4** the theoretical phase diagram of the model is depicted superimposing the training points (red dots) and the predicted phase transition lines (red lines). Note that the training data are only the red dots placed over the axis, while the prediction of the model corresponds to the whole plain. The appealing fact of this work is that only very few points were used over the $\kappa = 0$ or $h = 0$ axes but, nevertheless, the whole phase diagram, including the phase transition lines, was correctly reproduced. It is really remarkable the ability of the QCNN to disentangle the complete phase diagram, including the point with $h = 0$ and $\kappa = 0.5$ where three phases coexist. Note that in ref. [58], the unsupervised anomaly detection ML technique has also been used, but only a qualitative agreement is obtained to reproduce the phase diagram (Figure 4).

To finish this subsection, we can compare the two models analyzed. In both cases, the wave functions are generated in a quantum manner. In the case of the Agassi model the phase of the system is determined through the time evolution of a given state, while for the Ising model, it is done using a VQE. For the learning part, a CNN is constructed in the Agassi model, while in the Ising model a QCNN is employed. In both cases, the labeling of the classes is done thanks to the analytical knowledge of the phase diagram, although in the case of the Ising model this is true only for part of the phase diagram. In the Agassi model only supervised ML is used, while in the Ising case unsupervised ML (AD) is also considered, although only with qualitative results.

4.2. Shell Model Calculations: the Ground State of Nuclear Systems

The determination of the ground state of a nuclear system is one of the central problems of nuclear physics, as it is for quantum chemistry to determine the structure of a given molecule. The exact treatment of this problem is really far from our present knowledge, and consequently, the use of some kind of effective

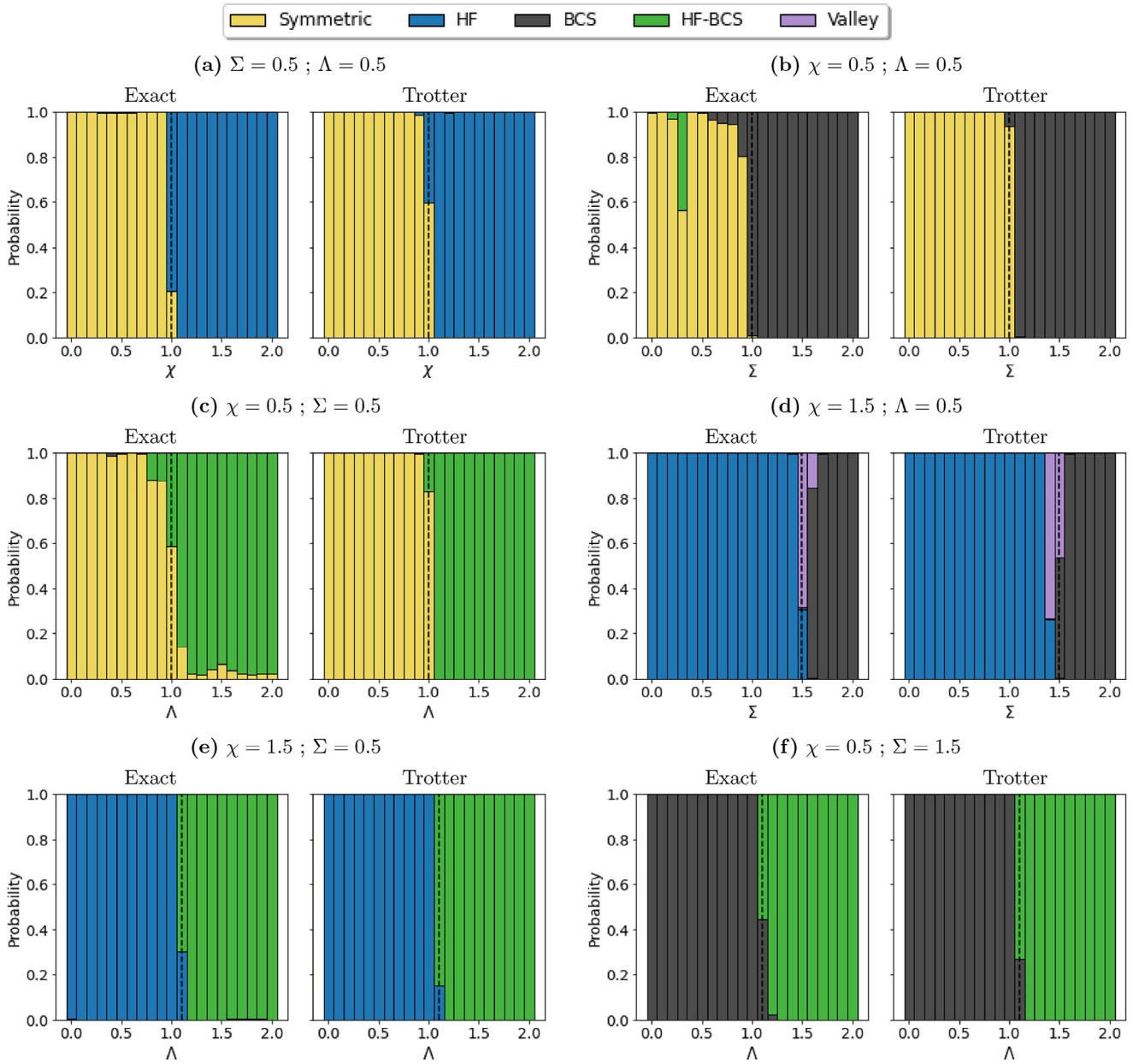

Figure 2. Quantum phase prediction of the system via the CNN. The graphs show the probability that the system is in a given phase for each point, predicted only from the time evolution of the $C_z(1, 2)$ correlation function; both the exact solution and the one obtained from the Trotter expansion with $n_T = 6$ are presented for the initial state $|\downarrow_1 \downarrow_2 \downarrow_3 \downarrow_4 \uparrow_5 \uparrow_6 \uparrow_7 \uparrow_8\rangle$ with $\epsilon = 1$. QPTs are shown moving through the following lines of the phase space: a) $\Sigma = 0.5$ and $\Lambda = 0.5$ moving from $\chi = 0$ (Symmetric) to $\chi = 2$ (HF - broken symmetry monopole–monopole induced Hartree-Fock type); b) $\chi = 0.5$ and $\Lambda = 0.5$ moving from $\Sigma = 0$ (Symmetric) to $\Sigma = 2$ (BCS - broken symmetry pairing induced BCS type); c) $\chi = 0.5$ and $\Sigma = 0.5$ moving from $\Lambda = 0$ (Symmetric) to $\Lambda = 2$ (Combined broken symmetry HF-BCS); d) $\chi = 1.5$ and $\Lambda = 0.5$ moving from $\Sigma = 0$ (HF) to $\Sigma = 2$ (BCS); e) $\chi = 1.5$ and $\Sigma = 0.5$ moving from $\Lambda = 0$ (HF) to $\Lambda = 2$ (Combined HF-BCS); (f) $\chi = 0.5$ and $\Sigma = 1.5$ moving from $\Lambda = 0$ (BCS) to $\Lambda = 2$ (Combined HF-BCS). See the text for the definition of the phases. The dashed black line in each graph denotes the theoretical critical point between phases for each case. Reproduced with permission.[51] Copyright 2022, American Physical Society.

model is required (see Section 2). One of these models is the nuclear shell model, which provides an ideal starting framework for quantum simulations. Below, different key examples of proposed quantum simulations to calculate ground state energies in nuclear systems are discussed. All of them correspond to the pioneering implementation of the VQE technique[26,27] to obtain the ground state of an atomic nucleus. The VQE is a variational procedure that strongly depends on the *ansatz* used. It is a hard problem to disentangle whether the trial state is the most appropriate or not. To help along this line, a work in which a reinforcement learning optimization approach is carried out over a variational quantum circuit[60] has been proposed. This method shows a very

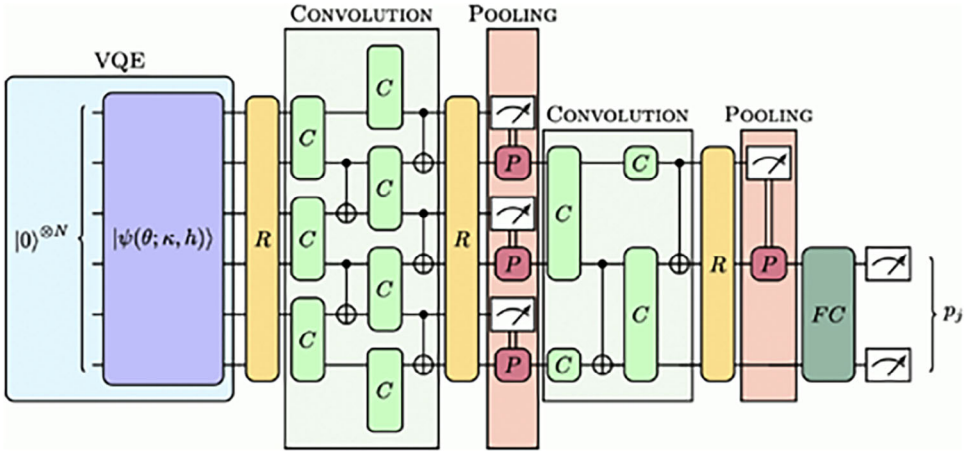

Figure 3. Circuit architecture: VQE states (blue) are the input of the quantum CNN composed of free rotations R (yellow), convolutions C (light green), pooling P (red), and a fully connected layer FC (dark green). Reproduced from ref. [58]. This figure is licensed under CC BY-SA 4.0.

remarkable performance in reproducing the ground state energy of the LiH molecule.

One of the first works in nuclear physics using the VQE was the study of the ground state structure of deuteron in a quantum computer discussed in ref. [24]. The deuteron was treated using a Hamiltonian extracted from a pionless effective field theory such that it can be simulated on a quantum chip. The ground state is obtained using a variational wave-function *ansatz* based on the unitary coupled-cluster theory (UCC). In the case of the deuteron, the dimension of the Hilbert space is very small and only three single-particle states have been considered. However, for the extrapolation to larger systems, the harmonic-oscillator variant of Lüscher's formula for finite-size corrections to the ground-state energy has been used and, as a result, the energy of the ground state is only 0.5% away from the exact value. The expectation value of the different terms appearing in the Hamiltonian and evaluated in two different quantum computers are presented in **Figure 5**. The θ variable in the X axis of Figure 5 is the corresponding variational parameter. This type of calculation opens the possibility of dealing with heavier systems that are not accessible via calculations on classical computers.

Another example of the use of the VQE is refs. [61, 62] where a widely used model that sketches the nuclear interaction, such as the LMG model,[19] was implemented in a quantum computer and the ground state was determined using the VQE. In this case, the design of the trial wave function is guided by symmetry considerations of the model and it makes possible to use a single variational parameter, θ, in the wave function for four particles, which is a rather good approximation,

$$|\psi(\theta)\rangle = \cos^2\theta|\downarrow\downarrow\downarrow\downarrow\rangle + \sin^2\theta|\uparrow\uparrow\uparrow\uparrow\rangle + -\frac{1}{\sqrt{12}}\sin 2\theta(|\uparrow\uparrow\downarrow\downarrow\rangle + |\downarrow\downarrow\uparrow\uparrow\rangle + |\downarrow\uparrow\downarrow\uparrow\rangle + |\downarrow\uparrow\uparrow\downarrow\rangle + |\uparrow\downarrow\downarrow\uparrow\rangle + |\uparrow\downarrow\uparrow\downarrow\rangle) \tag{10}$$

Also focused in the LMG model, in ref. [63] the equation of state method, which is an extension of the VQE, is employed to obtain excited states of the system. In this work, two levels of complexity were used, RPA (Random Phase Approximation) or second RPA (SRPA) and they found no noticeable difference between both. Therefore, RPA is the most appropriate choice. Other recent publications of interest include,[64] where the VQE is applied to the LMG and Agassi models, taking into account the symmetry of the problem to construct the variational wave function; as well as ref. [65], where the same strategy is applied to the $J_1 - J_2$ Heisenberg model.

So far, we have seen two types of approaches for defining the variational state, either using the UCC or using the symmetry of the Hamiltonian to guide the choice of the trial wave

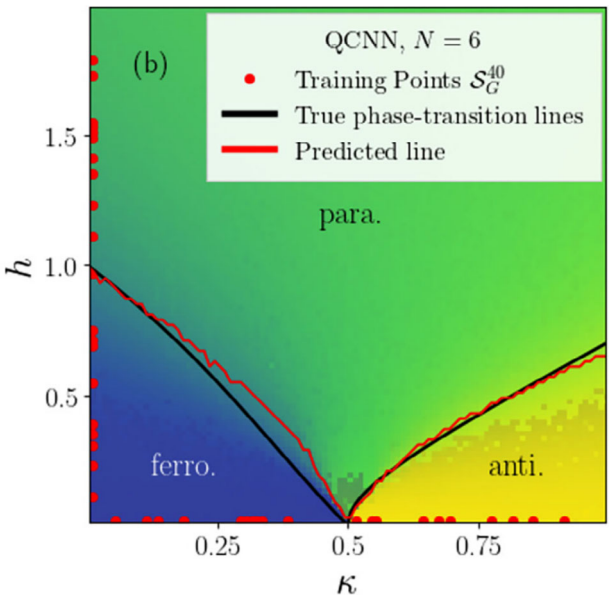

Figure 4. Phase diagram of the ANNNI model predicted by the trained QCNN for $N = 6$. Reproduced from ref. [58]. This figure is licensed under CC BY-SA 4.0.

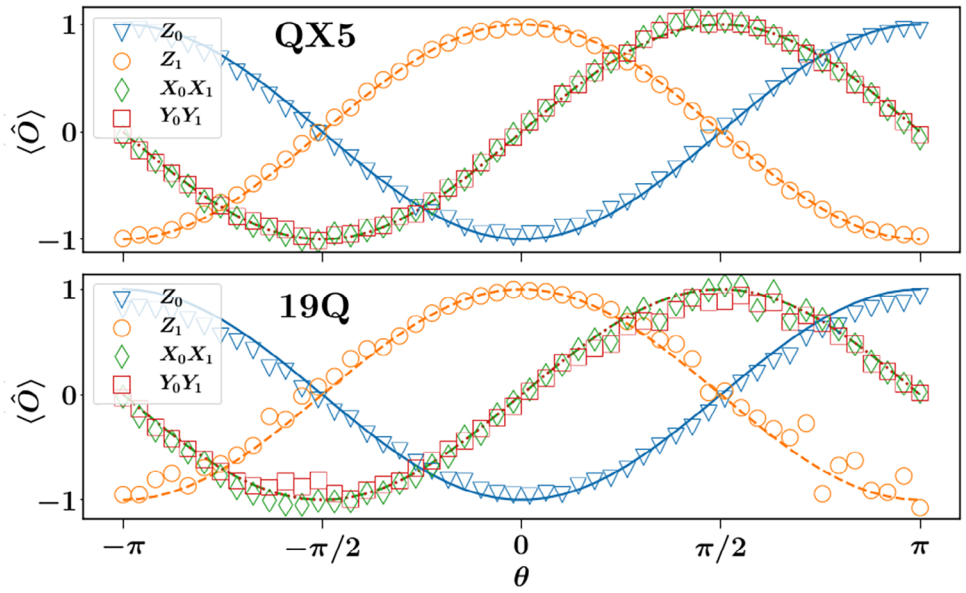

Figure 5. Experimentally determined energies for expectation values of the Pauli terms needed to calculate the ground state energy of deuteron as obtained on the QX5 and 19Q chips. Symbols stand for the experimental results, while lines stand for the theory. Reproduced with permission ref. [24]. Copyright 2018, American Physical Society.

function. In both cases, they were applied to small systems. Next, we will present in detail a set of works where the considered nuclei are heavier and, therefore, their Hilbert spaces are much larger. In these cases, the authors consider as trial wave function the UCC *ansatz* with Adaptive derivative-assembled problem-tailored (ADAPT)-VQE,[66] which seems to provide a clear advantage over other VQE approaches. In general, ADAPT-VQE is superior to the random or lexical ordering of the excitation operators in terms of convergence and circuit depth. The ADAPT-VQE defines the *ansatz* by selecting operators from a pool,

$$\{\hat{\tau}_1, \hat{\tau}_2, \ldots, \hat{\tau}_N\} \tag{11}$$

that presents the largest influence on the gradient, i.e., the largest value of

$$\left|\frac{\partial E}{\partial \theta_i}\right|_{\theta_i=0} = |\langle\psi|[H, \hat{\tau}_i]|\psi\rangle| \tag{12}$$

where H is the system Hamiltonian and θ_i correspond to the variational parameters. Once a new operator from the pool has been selected, k optimization steps of the ground state energy are carried out until convergence is reached, before moving to a new term from the pool. It is worth mentioning that with this method, the number of trainable parameters does not grow exponentially with the size of the system. The number and type of operators in the pool can be limited thanks to symmetry consideration, which can strongly reduce the complexity of the calculation. This method has been used for ^{6}Li,[67] reaching a precision for the energy of a 3.81% for the ground state (relative difference with the exact result, obtained through a direct diagonalization) and 0.12% for the first excited one. The calculation was run in the IBM Quantum 27 qubits architecture `ibmq_mumbai` using error mitigation. The authors noticed that because the number of nuclear states grows very rapidly with the number of valence nucleons, the scaling of the VQE application becomes unfeasible, needing the use of symmetry arguments to reduce the number of operators in the pool.

A step forward to improve the use of ADAPT-VQE is to start with a more correlated initial state, not just the Hartree-Fock one. In ref. [68], the authors use the UCC with ADAPT-VQE, but they include two-particle two-hole excitations in the initial state, obtaining a rather good approximation for the ground state energy of ^{6}He, ^{6}Be, ^{20}O and ^{22}O. In **Figure 6**, the circuit to implement a Hartree-Fock state including two-particle two-hole excitations is shown.

The latest case to be discussed[69,70] also corresponds to the use of ADAPT-VQE to obtain the ground state within the nuclear shell model, but in this case, the authors present a rather general formalism and a large set of potential nuclei can be considered. The formalism is intended to work in the p shell ($0p_{1/2}$, $0p_{3/2}$ orbitals), the sd shell ($1s_{1/2}$, $0d_{3/2}$, and $0d_{5/2}$ orbitals) or the pf shell ($0f_{7/2}$, $0f_{5/2}$, $1p_{3/2}$, and $1p_{1/2}$ orbitals). The number of single-particle states, either for protons or neutrons, are 6, 12, and 20, respectively. The type of two-body interaction to deal with the above shells is the Cohen-Kurath interaction in the p shell, the USDB in the sd shell and the KB3G interaction in the pf shell. The dimension of the Hilbert space will correspond to the product of the dimension of the states for protons and neutrons, which depend in a combinatorial way on the size of the single-particle space and the number of valence particles. This makes unfeasible a direct diagonalization when the dimension is well above of several millions, even using the Lanczos algorithm. Quantum computation has the capability to avoid this problem using the ADAPT-VQE approximation. The fermion nuclear shell model Hamiltonian is easily mapped into Pauli matrices using a Jordan-Wigner (JW) transformation. The JW mapping only requires as many qubits as single-particle states, independently of the

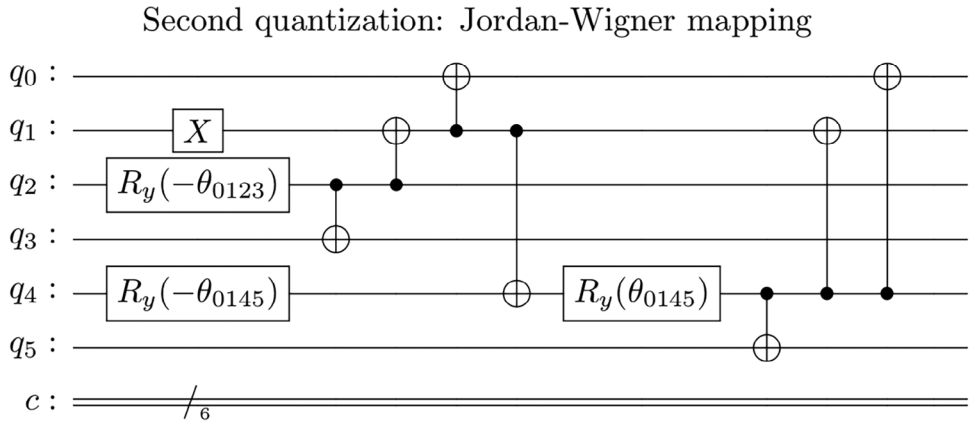

Figure 6. Circuit for including a limited number of two-particle, two-hole configurations on top of the Hartree-Fock solution for two particles in six states. Reproduced with permission.[68] Copyright 2022, American Physical Society.

number of valence particles, which means that the dimension of the problem remains constant for all nuclei belonging to the same major shell. In this work, the authors explore the complete quantum circuit design to estimate the necessary resources to carry out the nuclear shell-model calculations in regions where the standard approaches cannot be used. In **Figure 7**, a quantum circuit with five layers to prepare the ground state of the nucleus ^{18}O is shown. The multiqubit gates in boxes are defined as $U_{rs}^{pq}(\theta) = e^{i\theta T_{rs}^{pq}}$, where T_{rs}^{pq} is a two-particle promotion operator present in the pool of operators of the ADAPT-VQE method. The state defined in Figure 7 has an energy accuracy better than 10^{-6}.

An important conclusion of this work is that the accuracy for the ground state energy obtained with this approach is increasing faster than the growth of the number of CNOT gates. In **Figure 8**, the error value together with the number of used CNOT gates is depicted and one can easily note that the errors decay exponentially while the number of CNOT gates increases polynomially. The results obtained are very encouraging, having computed the ground state energy for ^{6}Be (10^{-8} relative error), ^{6}Li, ^{8,10}Be (10^{-7} relative error), ^{13}C (10^{-5} relative error), ^{18,19,20,22}O (10^{-6} relative error), ^{20,22,24}Ne (10^{-2} relative error), ^{42}Ca (10^{-8} relative error), and ^{44,46,48,50}Ca (10^{-2} relative error).

Finally, tightly connected with the use of the shell model or other simple models, there are a few other publications that deserve to be mentioned. In ref. [71] the comparison between the use of qubits and qudits is explored in the Agassi model. In ref. [72], the authors studied the effect of using effective model spaces in the quantum computation. In ref. [73], the authors calculate the position of the neutron drip line in oxygen isotopes employing a VQE. A quantum imaginary time evolution is used in ref. [74] to solve the Hartree-Fock equations. The issue of restoring symmetries or preparing states with a given symmetry is analyzed in depth in refs. [75–78]. Finally, in ref. [79], a technique for preparing excited states is presented and in ref. [80], a neutrino-nucleus scattering calculation has been implemented in a quantum computer. The work[81] is of particular interest, where a VQE entanglement forging based variational algorithm, employing generative neural networks, is used to obtain the ground-state

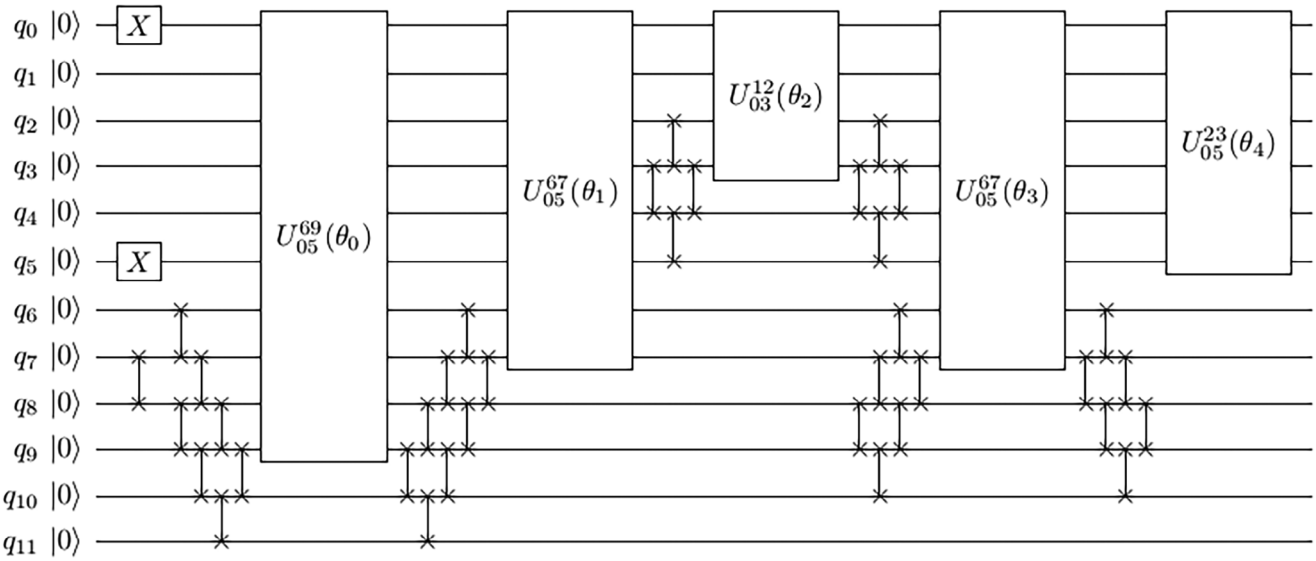

Figure 7. Circuit to prepare the ^{18}O ground state. Reproduced from ref. [69]. This figure is licensed under CC BY-SA 4.0.

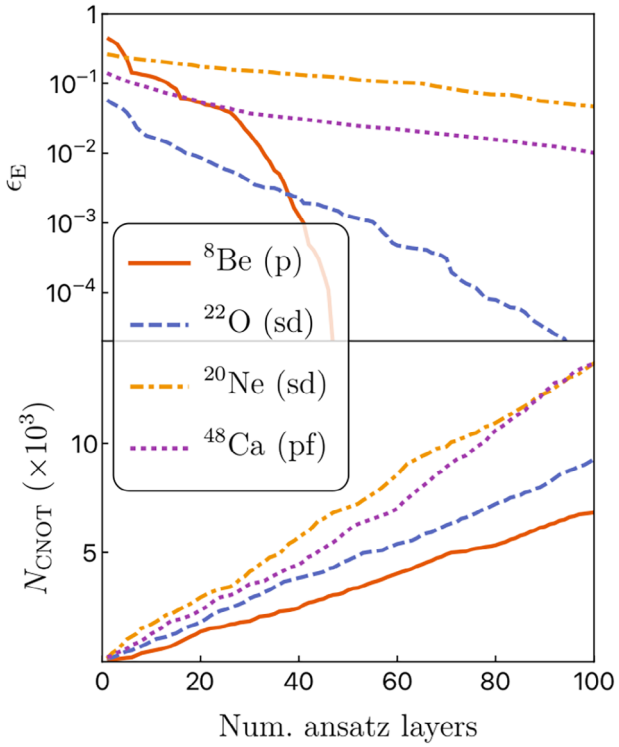

Figure 8. Evolution of the relative error for the ground-state energy (top panel) and number of CNOT gates (bottom panel) for selected examples. Reproduced from ref. [69]. This figure is licensed under CC BY-SA 4.0.

energy of several nuclei in the sd shell. The use of this method allows to reproduce the ground-state energy quite accurately while reducing the number of qubits needed.

4.3. Particle Identification and Track Reconstruction

The detection and identification of particles, including the measurements of their properties, such as energy, charge, linear, or angular momentum is the cornerstone of nuclear and high energy physics experiments since the pioneering works of E. Rutherford making collide α particles with a thin foil of gold until nowadays. Nuclear physics and high energy physics experiments present many aspects in common. In particular, the need to know the precise trajectory of the particle inside the detector system or the large number of events to be analyzed (much larger in the case of high energy physics) are standard tasks in the experiments of both research areas. In nuclear physics, γ-ray spectra is a standard technique for isotope identification and fundamental to nuclear structure studies. It is critical to determine the energy spectrum of the nuclei and to obtain information about transition probabilities between states, which is essential to disentangle the internal structure of the states. Also, the spectroscopy of charged particles, β or α, is of great relevance. So far, no QML techniques have been used in nuclear spectroscopy, but classical ML methods have already been applied (see Section 2.3). In particular, in ref. [82] the authors show that classical CNN and Transformer-Encoder methods outperforms deterministic algorithms in challenging classification problems in low-energy physics, such as distinguishing single from double β events. In high energy physics, practical examples of the application of QML already exist,[44,45] which could serve as inspiration for nuclear physics. On the one hand, the use of quantum generative models can gain some advantage over the classical ones due to the probabilistic character of quantum measurements. On the other hand, the analysis of data of quantum character, as the ones coming from nuclear physics, using QML is expected to be performed in a faster way than with classical ML. Here, we describe two QML techniques already applied to high energy physics that could be easily implemented in low-energy nuclear experiments.

The first example corresponds to the determination of the precise trajectory followed by a charged particle or a photon (which ionizes the active volume of the detector), which is commonly known as tracking. Tracking consists in associating the hits observed in the system of detectors to a given particle, and then, reconstructing its trajectory. Tracking is the cornerstone of particle path reconstruction, which is compulsory to identify the nature of events of interest. In high luminosity experiments, as happens with LHC experiments, the number of events to be analyzed is really large and, therefore, to carry out the tracking of particles becomes a challenge. Nowadays, state-of-the-art algorithms are based on the use of Kalman filters. This approach is rather reliable and robust, providing good physics performance. Its main problem is related to its scalability, which is expected to be worse than quadratic with the increase in the number of simultaneous collisions. Therefore, it is of great interest to explore other approaches to speed up the process, including deep machine learning techniques. Such a new avenue is based on image-based interpretation of the detector data where the use of CNN could provide high-accuracy results. The HEPtrkX project[83] and its evolution, EXAtrkX,[84] followed this approach and it is based on graph neural networks (GNNs) to perform hits and segments classification.

A step further corresponds to the use of a GNN architecture from a quantum computing perspective, implementing the original networks as quantum circuits.[85] In this work, the analysis begins with the TrackML dataset,[86] a publicly available dataset that consists of simulated measurements of many detector layers in a cylindrical geometry. The detector layers are arranged using a model layout that is common to most LHC experiments. This set of data is first preprocessed prior to the training. The HepTrkX team proposed a GNN to perform segment classification. The model consists of three types of networks. The first one is an input network, the second one is the edge network and the third one is the node network. The model has an overall accuracy of 99.5% in correctly identifying the track.

To transform the GNN into a quantum circuit, many modifications are needed. For simplicity, the authors only take into account the edge network and do not use the input and the node networks. Next, the Tree Tensor Network (TTN) is considered among the hierarchical quantum classifiers as the quantum circuit to replace the neural network layer. The input (taken from the TrackML dataset) is encoded in qubits and then the TTN circuit is applied. The TTN circuit is composed of R_y and CNOT gates. R_y gates start with random parameters that will be tuned later. The CNOT gate is used to introduce correlations between qubits so that their values are not independent. At the end of the circuit, there is a measurement. The structure of the quantum circuit is

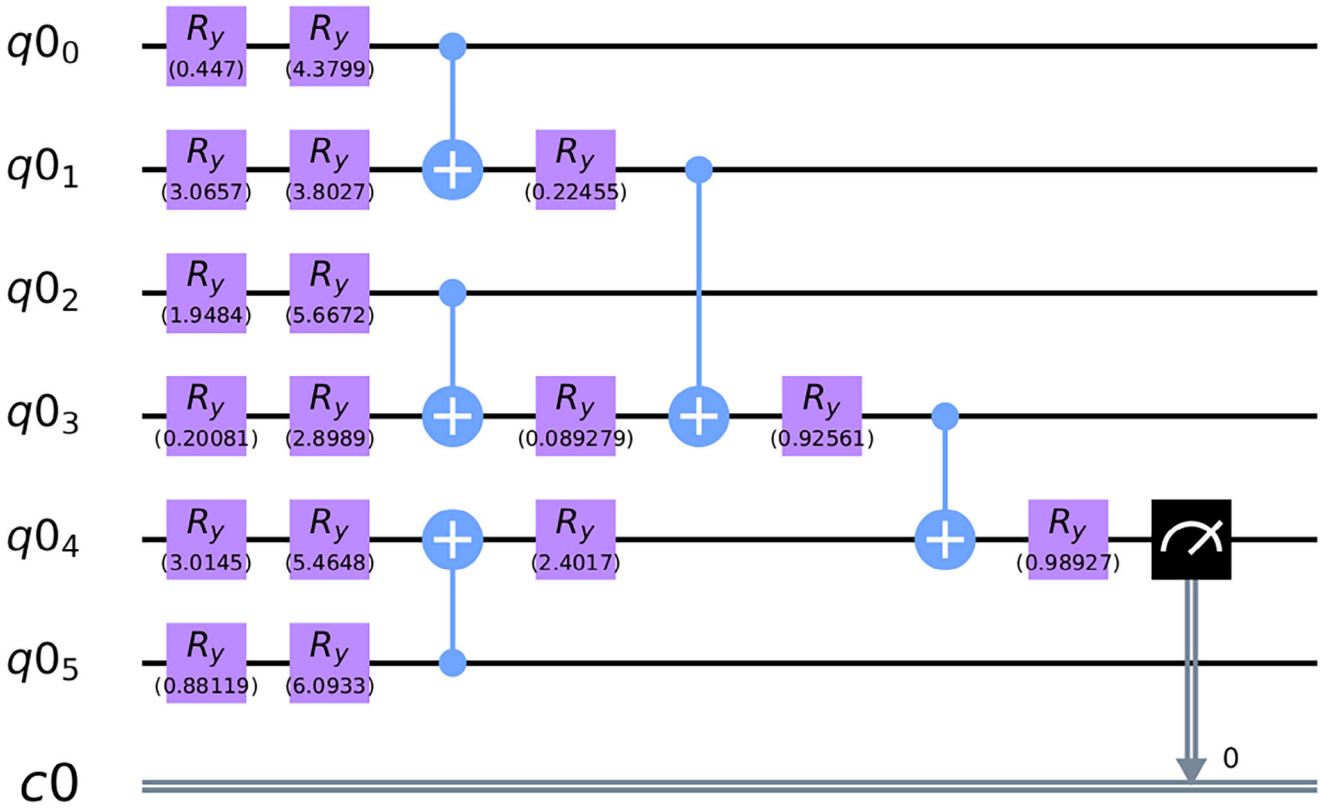

Figure 9. Qubit tree tensor network (TTN) representation of the Quantum Edge Network. Reproduced from ref. [85]. This figure is licensed under CC BY-SA 4.0.

depicted in **Figure 9**. The quantum circuit was trained over two epochs. This low number is used to simplify as much as possible the quantum circuit. The data were divided randomly into training and test sets with a ratio of 9 to 1. The model is trained using stochastic gradient descent and weighted binary cross entropy. The training performance of the model can be seen in **Figure 10**. Note that the accuracy obtained is noticeably small, but this is mainly due to the oversimplification of the model. At the end of the day, this is still a proof-of-principle prototype of a complete quantum GNN structure.

The second example that we will present corresponds to the application of QML to identify if a jet contains a hadron formed by a b (bottom) or $\bar{b}$ quark[87] at the moment of production. To this end, the Variational Quantum Classifier (VQC) is used with simulated data from the LHCb experiment. LHCb is a single-arm spectrometer designed to study b and c (charm) hadrons

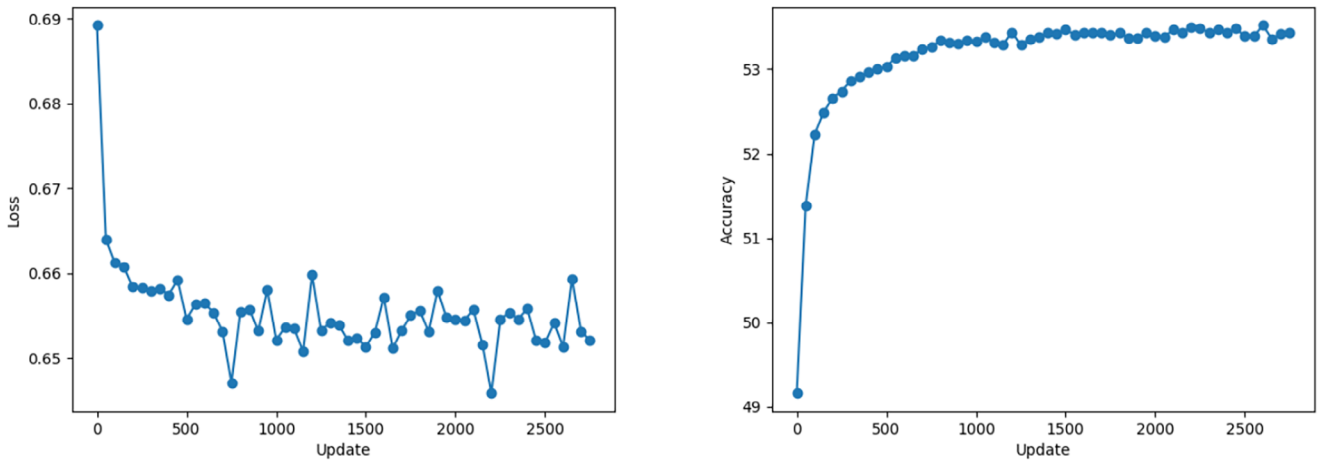

Figure 10. Training loss (on the left) and validation accuracy (on the right) of the TTN in two full epochs. Reproduced from ref. [85]. This figure is licensed under CC BY-SA 4.0.

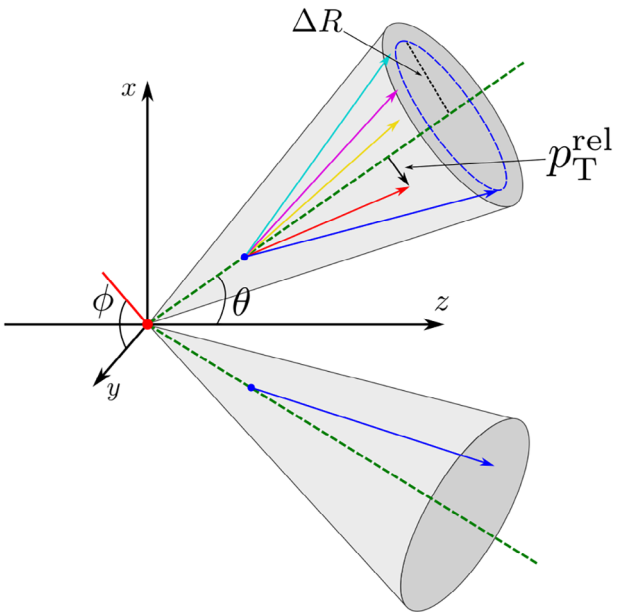

Figure 11. Schematic representation of the two jet tagging methods. In the exclusive method, the information comes from a particle and a muon (lower jet); in the inclusive method, the information is extracted from the jet constituents (upper jet). Reproduced from ref. [87]. This figure is licensed under CC BY-SA 4.0.

in the forward region of proton–proton collisions. The analysis is restricted to a sample of jets that belong to these two categories, labeled either as b jets or as $\bar{b}$ jets. Hence, we have a binary classification problem. The QML approach presented in this application belongs to the category of inclusive algorithms (upper jet of **Figure 11**, i.e., the information is extracted from the jet constituents). The figure of merit of this work corresponds to the tagging power, defined as

$$\epsilon_{tag} = \epsilon_{eff}(2a-1)^2 \tag{13}$$

where ϵ_{eff} is the tagging efficiency and a the accuracy, i.e., the fraction of correctly tagged jets with respect to the tagged jets.

The QML procedure is implemented with a VQC which is a hybrid quantum-classical algorithm to perform classification tasks based on a Parametrized Quantum Circuit (PQC). The structure of the PQC consists in i) the data encoding, ii) the variational circuit and, iii) the prediction. Two different PQCs are used in this work, the Amplitude Embedding and the Angle Embedding. In **Figure 12**, we depict the quantum circuit for the first case. The probability of identifying a b or a $\bar{b}$ is connected with the measurement of σ_z, i.e. $\langle\sigma_z\rangle$.

In this work, two different datasets are used, namely, the muon and the complete one. As usual, both are split into training and testing sub-datasets: about 60% of the samples are used in the training and the remaining 40% are used to test, evaluate and compare the classifiers.

In **Figure 13**, the value of the tagging power as a function of jet p_T and η parameters is presented for the classical and quantum classifiers. The results are similar for the different classifiers, without any obvious bias. The tagging power decreases as the p_T value increases because for larger values of p_T the identification is more difficult. The deep neural network (DNN) shows slightly better performance compared to the Angle Embedding algorithm. In any case, both algorithms reach better results than the Amplitude Embedding model and the muon tagging approach.

An additional analysis of the value of the tagging power as a function of the number of training events shows that, for a large number of events, the performance of the quantum algorithm is similar to the DNN, but when the number of training events decreases, the quantum algorithm keeps very high performance, while the DNN is not able to perform a good classification. Therefore, with respect to the DNN, the QML method reaches optimal performance with a lower number of events (see **Figure 14**). This special feature of QML algorithms deserves an analysis in depth.

It is worth mentioning the two recent works[88,89] where the reconstruction of trajectories is formulated in terms of a quadratic unconstrained binary optimization (QUBO). This way, one can group two or three hits from consecutive detector layers and binary values represent if a given doublet or triplet corresponds to a particle track. In general, one has to build a QUBO Hamiltonian and its ground state will correspond to the desired solution.

5. Conclusion and Outlook

The field of nuclear physics, especially in the study of low-energy phenomena, is still in its infancy concerning the utilization of quantum computing. Although machine learning techniques

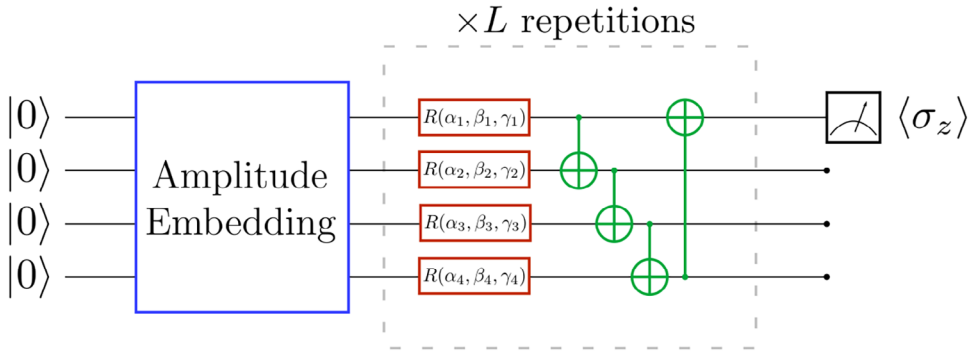

Figure 12. Circuit representation of the Amplitude Embedding model. In blue, variables that are embedded into the amplitudes of a quantum state. In red, trainable gates. In green, CNOT gates entangling qubits with a circular topology. Reproduced from ref. [87]. This figure is licensed under CC BY-SA 4.0.

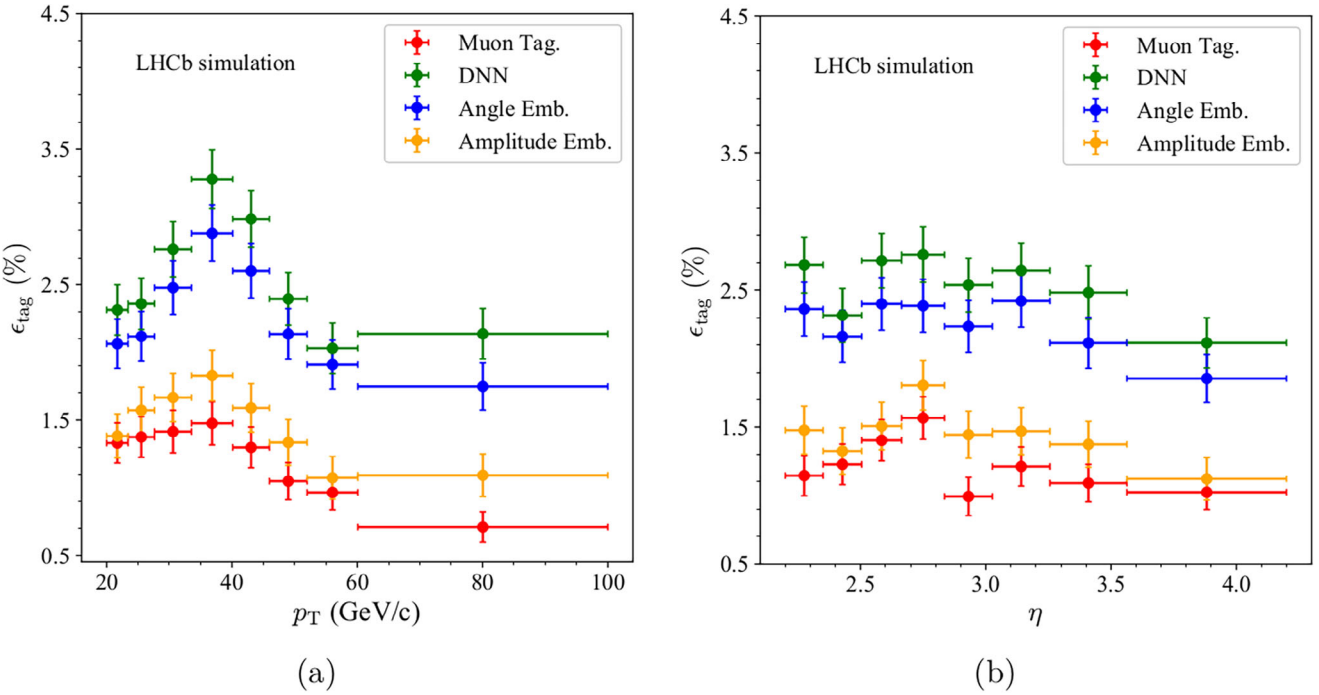

Figure 13. Tagging power ϵ_{tag} with respect to (a) jet p_T and (b) jet η for the muon dataset. Reproduced from ref. [87]. This figure is licensed under CC BY-SA 4.0.

have found extensive application in nuclear physics, the exploration of Quantum Machine Learning (QML) in the context of low-energy nuclear physics remains largely uncharted. This creates a significant gap in the scientific literature.

The aim of this perspective is to provide non-experts with essential insights to comprehend the current research landscape in nuclear structure studies and to introduce three noteworthy applications of quantum computing and QML in the realm of nuclear physics. The envisioned outcome is to inspire future research efforts. The three applications considered are: i) determining the phase and shape of a simplified nuclear system, ii) calculating the ground state of a system using a shell model Hamiltonian, and iii) identifying particle trajectories and particles in nuclear experiments.

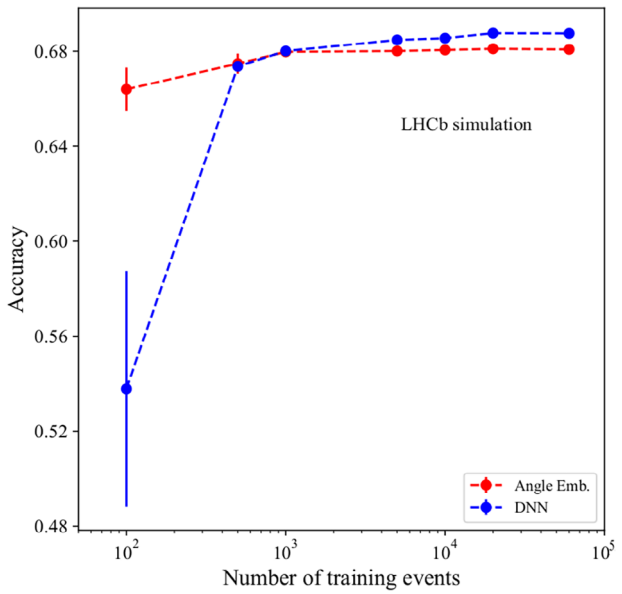

Figure 14. Accuracy of the (red) Angle Embedding structure and (blue) DNN on the muon dataset versus the number of training events. Reproduced from ref. [87]. This figure is licensed under CC BY-SA 4.0.

Acknowledgements

This work was partially supported by the Consejería de Universidad, Investigación e Innovación de la Junta de Andalucía (Spain) under Groups FQM-160, FQM-177, and FQM-370, and under projects P20-00617, P20-00764, P20-01247, and US-1380840; by grants PID2019-104002GB-C21, PID2019-104002GB-C22, PID2020-114687GB-I00, PID2022-136228NB-C21 and PID2022-136228NB-C22 funded by MCIN/AEI/10.13039/50110001103 and "ERDF A way of making Europe". This work has also been financially supported by the Ministry for Digital Transformation and of Civil Service of the Spanish Government through the QUANTUM ENIA project call - Quantum Spain project, and by the European Union through the Recovery, Transformation and Resilience Plan - NextGenerationEU within the framework of the "Digital Spain 2026 Agenda".

Conflict of Interest

The authors declare no conflict of interest.

Keywords

nuclear models, quantum machine learning, quantum phase transitions

Received: July 14, 2023
Revised: March 25, 2024
Published online:

[1] M. A. Nielsen, I. L. Chuang, *Quantum Computation and Quantum Information: 10th Anniversary Edition*, Cambridge University Press, Cambridge **2010**.
[2] J. Carlson, D. J. Dean, M. Hjorth-Jensen, D. Kaplan, J. Preskill, K. Roche, M. J. Savage, M. Troyer, *Quantum Computing for Theoretical Nuclear Physics, A White Paper prepared for the U.S. Department of Energy, Office of Science, Office of Nuclear Physics* **2018**, https://www.osti.gov/biblio/1631143.
[3] I. C. Cloët, M. R. Dietrich, J. Arrington, A. Bazavov, M. Bishof, A. Freese, A. V. Gorshkov, A. Grassellino, K. Hafidi, Z. Jacob, M. McGuigan, Y. Meurice, Z.-E. Meziani, P. Mueller, C. Muschik, J. Osborn, M. Otten, P. Petreczky, T. Polakovic, A. Poon, R. Pooser, A. Roggero, M. Saffman, B. VanDevender, J. Zhang, E. Zohar, *Opportunities for Nuclear Physics & Quantum Information Science* **2019**, https://doi.org/10.48550/arXiv.1903.05453.
[4] T. S. Humble, A. Delgado, R. Pooser, C. Seck, R. Bennink, V. Leyton-Ortega, C. C. J. Wang, E. Dumitrescu, T. Morris, K. Hamilton, D. Lyakh, P. Date, Y. Wang, N. A. Peters, K. J. Evans, M. Demarteau, A. McCaskey, T. Nguyen, S. Clark, M. Reville, A. D. Meglio, M. Grossi, S. Vallecorsa, K. Borras, K. Jansen, D. Krücker, *Snowmass White Paper: Quantum Computing Systems and Software for High-Energy Physics Research* **2022**, https://doi.org/10.48550/arXiv.2203.07091.
[5] D. Beck, J. Carlson, Z. Davoudi, J. Formaggio, S. Quaglioni, M. Savage, J. Barata, T. Bhattacharya, M. Bishof, I. Cloet, A. Delgado, M. DeMarco, C. Fink, A. Florio, M. Francois, D. Grabowska, S. Hoogerheide, M. Huang, K. Ikeda, M. Illa, K. Joo, D. Kharzeev, K. Kowalski, W. K. Lai, K. Leach, B. Loer, I. Low, J. Martin, D. Moore, T. Mehen, et al., Quantum Information Science and Technology for Nuclear Physics. Input into U.S. Long-Range Planning, 2023, **2023**, https://doi.org/10.48550/arXiv.2303.00113.
[6] K. Heyde, *Basic Ideas and Concepts in Nuclear Physics: An Introductory Approach*, Third Edition. Reino Unido, CRC Press, Boca Raton, FL **2020**.
[7] P. Ring, P. Schuck, *The Nuclear Many-Body Problem*, Springer, Berlin **2004**.
[8] L. M. Robledo, T. R. Rodríguez, R. R. Rodríguez-Guzmán, *J. Phys. G: Nucl. Part. Phys.* **2018**, *46*, 013001.
[9] A. Bohr, B. Mottelson, *Nuclear Structure*, vol *2*, W.AA. Benjamin, Inc, Reading, Massachusetts, London **1975**.
[10] D. Rowe, *Nuclear Collective Motion: Models and Theory*, World Scientific, Singapore **2010**.
[11] I. Talmi, *Simple Models of Complex Nuclei*, Harwood Academy Publication, New York **1993**.
[12] T. Niksic, D. Vretenar, P. Ring, *Prog. Part. Nucl. Phys.* **2011**, *66*, 519.
[13] M. Grasso, *Prog. Part. Nucl. Phys.* **2019**, *106*, 256.
[14] K. Kumar, M. Baranger, *Nucl. Phys. A* **1967**, *92*, 608.
[15] M. Baranger, K. Kumar, *Nucl. Phys. A* **1968**, *110*, 490.
[16] K. Kumar, M. Baranger, *Nucl. Phys. A* **1968**, *110*, 529.
[17] S. Koonin, D. Dean, K. Langanke, *Phys. Rep.* **1997**, *278*, 1.
[18] T. Otsuka, M. Honma, T. Mizusaki, N. Shimizu, Y. Utsuno, *Prog. Part. Nucl. Phys.* **2001**, *47*, 319.
[19] H. Lipkin, N. Meshkov, A. Glick, *Nucl. Phys.* **1965**, *62*, 188.
[20] D. Agassi, *Nucl. Phys. A* **1968**, *116*, 49.
[21] R. Richardson, *Phys. Lett.* **1963**, *3*, 277.
[22] J. Dukelsky, S. Pittel, G. Sierra, *Rev. Mod. Phys.* **2004**, *76*, 643.
[23] I. M. Georgescu, S. Ashhab, F. Nori, *Rev. Mod. Phys.* **2014**, *86*, 153.
[24] E. F. Dumitrescu, A. J. McCaskey, G. Hagen, G. R. Jansen, T. D. Morris, T. Papenbrock, R. C. Pooser, D. J. Dean, P. Lougovski, *Phys. Rev. Lett.* **2018**, *120*, 210501.
[25] T. Ayral, P. Besserve, D. Lacroix, E. A. Ruiz Guzman, *Eur. Phys. J. A* **2023**, *59*, 227.
[26] A. Peruzzo, J. McClean, P. Shadbolt, M.-H. Yung, X.-Q. Zhou, P. J. Love, A. Aspuru-Guzik, J. L. O'Brien, *Nat. Commun.* **2014**, *5*, 4213.
[27] J. Tilly, H. Chen, S. Cao, D. Picozzi, K. Setia, Y. Li, E. Grant, L. Wossnig, I. Rungger, G. H. Booth, J. Tennyson, *Phys. Rep.* **2022**, *986*, 1.
[28] V. Dunjko, H. J. Briegel, *Rep. Prog. Phys.* **2018**, *81*, 074001.
[29] J. Biamonte, P. Wittek, N. Pancotti, P. Rebentrost, N. Wiebe, S. Lloyd, *Nature* **2017**, *549*, 195.
[30] A. Boehnlein, M. Diefenthaler, N. Sato, M. Schram, V. Ziegler, C. Fanelli, M. Hjorth-Jensen, T. Horn, M. P. Kuchera, D. Lee, W. Nazarewicz, P. Ostroumov, K. Orginos, A. Poon, X.-N. Wang, A. Scheinker, M. S. Smith, L.-G. Pang, *Rev. Mod. Phys.* **2022**, *94*, 031003.
[31] H. GM, M. K. Gourisaria, M. Pandey, S. S. Rautaray, *Comp. Sci. Rev.* **2020**, *38*, 100285.
[32] D. Guest, K. Cranmer, D. Whiteson, *Annu. Rev. Nucl. Part. Sci.* **2018**, *68*, 161.
[33] P. T. Komiske, E. M. Metodiev, M. D. Schwartz, *J. High Energy Phys.* **2017**, *2017*, 110.
[34] C. Fanelli, J. Pomponi, *Mach. Learn.: Sci. Technol.* **2020**, *1*, 015010.
[35] R. Barsotti, M. Shepherd, *J. Instrum.* **2020**, *15*, P05021.
[36] C. W. Bauer, Z. Davoudi, N. Klco, M. J. Savage, *Nat. Rev. Phys.* **2023**, *5*, 420.
[37] L. Lamata, A. Parra-Rodriguez, M. Sanz, E. Solano, *Adv. Phys.: X* **2018**, *3*, 1457981.
[38] G. H. Low, I. L. Chuang, *Phys. Rev. Lett.* **2017**, *118*, 010501.
[39] L. Gui-Lu, *Commun. Theor. Phys.* **2006**, *45*, 825.
[40] C. Gyurik, V. Dunjko, On establishing learning separations between classical and quantum machine learning with classical data, **2023**, https://arxiv.org/abs/2208.06339.
[41] L. Lamata, *Adv. Quantum Technol.* **2023**, *6*, 2300059.
[42] X. Pan, Z. Lu, W. Wang, Z. Hua, Y. Xu, W. Li, W. Cai, X. Li, H. Wang, Y.-P. Song, C.-L. Zou, D.-L. Deng, L. Sun, *Nat. Commun.* **2023**, *14*, 4006.
[43] L. Lamata, *Mach. Learn.: Sci. Technol.* **2020**, *1*, 033002.
[44] W. Guan, G. Perdue, A. Pesah, M. Schuld, K. Terashi, S. Vallecorsa, J.-R. Vlimant, *Mach. Learn.: Sci. Technol.* **2021**, *2*, 011003.
[45] A. D. Meglio, K. Jansen, I. Tavernelli, C. Alexandrou, S. Arunachalam, C. W. Bauer, K. Borras, S. Carrazza, A. Crippa, V. Croft, R. de Putter, A. Delgado, V. Dunjko, D. J. Egger, E. Fernandez-Combarro, E. Fuchs, L. Funcke, D. Gonzalez-Cuadra, M. Grossi, J. C. Halimeh, Z. Holmes, S. Kuhn, D. Lacroix, R. Lewis, D. Lucchesi, M. L. Martinez, F. Meloni, A. Mezzacapo, S. Montangero, L. Nagano, et al., Quantum computing for high-energy physics: State of the art and challenges. summary of the qc4hep working group, **2023**, https://doi.org/10.48550/arXiv.2307.03236.
[46] M. L. Olivera-Atencio, L. Lamata, J. Casado-Pascual, *Adv. Quantum Technol.* **2023**, 2300247.
[47] S. Sachdev, *Quantum Phase Transitions*, Cambridge University Press, Cambridge, UK **2011**.
[48] F. Iachello, A. Arima, *The Interacting Boson Model*, Cambridge Monographs on Mathematical Physics, Cambridge University Press, Cambridge **1987**.
[49] L. Landau, E. Lifshitz, *Statistical Physics*, Pergamon Press, Oxford **1969**.
[50] F. Iachello, N. V. Zamfir, R. F. Casten, *Phys. Rev. Lett.* **1998**, *81*, 1191.
[51] A. Sáiz, J. E. García-Ramos, J. M. Arias, L. Lamata, P. Pérez-Fernández, *Phys. Rev. C* **2022**, *106*, 064322.
[52] P. Pérez-Fernández, J.-M. Arias, J.-E. García-Ramos, L. Lamata, *Phys. Lett. B* **2022**, *829*, 137133.

[53] J. E. García-Ramos, J. Dukelsky, P. Pérez-Fernández, J. M. Arias, *Phys. Rev. C* **2018**, *97*, 054303.
[54] E. D. Davis, W. D. Heiss, *J. Phys. G: Nucl. Phys.* **1986**, *12*, 805.
[55] C. D. Batista, G. Ortiz, *Phys. Rev. Lett.* **2001**, *86*, 1082.
[56] P. Jordan, E. Wigner, *Zeitschrift für Physik* **1928**, *47*, 631.
[57] F. Iachello, N. V. Zamfir, *Phys. Rev. Lett.* **2004**, *92*, 212501.
[58] S. Monaco, O. Kiss, A. Mandarino, S. Vallecorsa, M. Grossi, *Phys. Rev. B* **2023**, *107*, L081105.
[59] M. Cea, M. Grossi, S. Monaco, E. Rico, L. Tagliacozzo, S. Vallecorsa, Exploring the phase diagram of the quantum one-dimensional annni model, **2024**, https://arxiv.org/abs/2402.11022.
[60] M. Ostaszewski, L. M. Trenkwalder, W. Masarczyk, E. Scerri, V. Dunjko, In M. Ranzato, A. Beygelzimer, Y. Dauphin, P. Liang, J. W. Vaughan, *Advances in Neural Information Processing Systems*, vol. *34*, Curran Associates, Inc, Scotland **2021**, pp. 18182–18194.
[61] M. J. Cervia, A. B. Balantekin, S. N. Coppersmith, C. W. Johnson, P. J. Love, C. Poole, K. Robbins, M. Saffman, *Phys. Rev. C* **2021**, *104*, 024305.
[62] M. Q. Hlatshwayo, J. Novak, E. Litvinova, Quantum benefit of the quantum equation of motion for the strongly coupled many-body problem, **2023**, https://doi.org/10.48550/arXiv.2309.10179.
[63] M. Q. Hlatshwayo, Y. Zhang, H. Wibowo, R. LaRose, D. Lacroix, E. Litvinova, *Phys. Rev. C* **2022**, *106*, 024319.
[64] J. Gibbs, Z. Holmes, P. Stevenson, Exploiting symmetries in nuclear hamiltonians for ground state preparation, **2024**, https://arxiv.org/abs/2402.10277.
[65] G. Crognaletti, G. D. Bartolomeo, M. Vischi, L. L. Viteritti, Equivariant variational quantum eigensolver to detect phase transitions through energy level crossings, **2024**, https://arxiv.org/abs/2403.07100.
[66] H. R. Grimsley, S. E. Economou, E. Barnes, N. J. Mayhall, *Nat. Commun.* **2019**, *10*, 3007.
[67] O. Kiss, M. Grossi, P. Lougovski, F. Sanchez, S. Vallecorsa, T. Papenbrock, *Phys. Rev. C* **2022**, *106*, 034325.
[68] I. Stetcu, A. Baroni, J. Carlson, *Phys. Rev. C* **2022**, *105*, 064308.
[69] A. Pérez-Obiol, A. M. Romero, J. Menéndez, A. Rios, A. García-Sáez, B. Juliá-Díaz, *Sci. Rep.* **2023**, *13*, 12291.
[70] A. M. Romero, J. Engel, H. L. Tang, S. E. Economou, *Phys. Rev. C* **2022**, *105*, 064317.
[71] M. Illa, C. E. P. Robin, M. J. Savage, Quantum Simulations of SO(5) Many-Fermion Systems using Qudits, **2023**, https://doi.org/10.48550/arXiv.2305.11941.
[72] C. E. P. Robin, M. J. Savage, *Phys. Rev. C* **2023**, *108*, 024313.
[73] C. Sarma, O. D. Matteo, A. Abhishek, P. C. Srivastava, Prediction of the neutron drip line in oxygen isotopes using quantum computation, **2023**, https://doi.org/10.48550/arXiv.2306.06432.
[74] Y. H. Li, J. Al-Khalili, P. Stevenson, A quantum simulation approach to implementing nuclear density functional theory via imaginary time evolution, **2023**, https://doi.org/10.48550/arXiv.2308.15425.
[75] D. Lacroix, *Phys. Rev. Lett.* **2020**, *125*, 230502.
[76] E. A. Ruiz Guzman, D. Lacroix, *Phys. Rev. C* **2022**, *105*, 024324.
[77] E. A. R. Guzman, D. Lacroix, *Phys. Rev. C* **2023**, *107*, 034310.
[78] D. Lacroix, E. A. Ruiz Guzman, P. Siwach, *Eur. Phys. J. A* **2023**, *59*, 3.
[79] A. Roggero, C. Gu, A. Baroni, T. Papenbrock, *Phys. Rev. C* **2020**, *102*, 064624.
[80] A. Roggero, A. C. Y. Li, J. Carlson, R. Gupta, G. N. Perdue, *Phys. Rev. D* **2020**, *101*, 074038.
[81] P. de Schoulepnikoff, O. Kiss, S. Vallecorsa, G. Carleo, M. Grossi, Hybrid ground-state quantum algorithms based on neural Schrödinger forging, **2023**, https://arxiv.org/abs/2307.02633.
[82] R. Moretti, M. Rossi, M. Biassoni, A. Giachero, M. Grossi, D. Guffanti, D. Labranca, F. Terranova, S. Vallecorsa, Assessment of few-hits machine learning classification algorithms for low energy physics in liquid argon detectors, **2024**, https://arxiv.org/abs/2305.09744.
[83] S. Farrell, D. Anderson, P. Calafiura, G. Cerati, L. Gray, J. Kowalkowski, M. Mudigonda, Prabhat, P. Spentzouris, M. Spiropoulou, A. Tsaris, J.-R. Vlimant, S. Zheng, *EPJ Web Conf.* **2017**, *150*, 00003.
[84] X. Ju, D. Murnane, P. Calafiura, N. Choma, S. Conlon, S. Farrell, Y. Xu, M. Spiropulu, J.-R. Vlimant, A. Aurisano, J. Hewes, G. Cerati, L. Gray, T. Klijnsma, J. Kowalkowski, M. Atkinson, M. Neubauer, G. DeZoort, S. Thais, A. Chauhan, A. Schuy, S.-C. Hsu, A. Ballow, A. Lazar, *Eur. Phys. J. C* **2021**, *81*, 876.
[85] C. Tüysüz, F. Carminati, B. Demirköz, D. Dobos, F. Fracas, K. Novotny, K. Potamianos, S. Vallecorsa, J.-R. Vlimant, *EPJ Web Conf.* **2020**, *245*, 09013.
[86] S. Amrouche, L. Basara, P. Calafiura, V. Estrade, S. Farrell, D. R. Ferreira, L. Finnie, N. Finnie, C. Germain, V. V. Gligorov, T. Golling, S. Gorbunov, H. Gray, I. Guyon, M. Hushchyn, V. Innocente, M. Kiehn, E. Moyse, J.-F. Puget, Y. Reina, D. Rousseau, A. Salzburger, A. Ustyuzhanin, J.-R. Vlimant, J. S. Wind, T. Xylouris, Y. Yilmaz, in *The NeurIPS '18 Competition*, (Eds.: S. Escalera, R. Herbrich), Springer International Publishing, Cham **2020**, pp. 231–264.
[87] A. Gianelle, P. Koppenburg, D. Lucchesi, D. Nicotra, E. Rodrigues, L. Sestini, J. de Vries, D. Zuliani, *J. High Energy Phys.* **2022**, *2022*, 14.
[88] A. Crippa, L. Funcke, T. Hartung, B. Heinemann, K. Jansen, A. Kropf, S. Kühn, F. Meloni, D. Spataro, C. Tüysüz, Y. C. Yap, Quantum algorithms for charged particle track reconstruction in the luxe experiment, **2023**, https://doi.org/10.48550/arXiv.2304.01690.
[89] T. Schwägerl, C. Issever, K. Jansen, T. J. Khoo, S. Kühn, C. Tüysüz, H. Weber, Particle track reconstruction with noisy intermediate-scale quantum computers, **2023**, https://doi.org/10.48550/arXiv.2303.13249.

José-Enrique García-Ramos is a full professor of nuclear physics at the Department of Integrated Sciences of the University of Huelva, Spain. Before working in Huelva, he was a postdoctoral fellow at the University of Gent, Belgium. Previously, he carried out his PhD at the University of Sevilla, Spain. Among his research interests, one can highlight the nuclear structure studies using algebraic methods, with emphasis in the nuclear shape-coexistence phenomena, the analysis of quantum phase transitions in nuclear systems and, finally, the use of quantum computing and quantum information concepts to solve nuclear problems.

Álvaro Sáiz is a Ph.D. student and researcher at Universidad de Sevilla in Spain. He graduated in Physics at the University of the Basque Country and then obtained his Masters degree in Astrophysics at the Universidad Complutense de Madrid.

José M. Arias is a Full Professor at the Department of Atomic, Molecular, and Nuclear Physics at the University of Sevilla, Spain. He completed his doctoral studies at several renowned institutions, including KVI in The Netherlands, Yale University in the United States, and the University of Sevilla in Spain, ultimately defending his doctoral thesis at the latter institution in 1985. He is particularly interested on nuclear and molecular structure studies, leveraging algebraic methods. He has also made contributions to the study of nuclear reaction mechanisms, and the analysis of quantum phase transitions in nuclear systems. In recent years, he has explored the application of quantum computing and quantum information concepts to address complex problems in the realm of nuclear physics.

Lucas Lamata is an associate professor (Profesor Titular de Universidad) of theoretical physics at the Departamento de Física Atómica, Molecular y Nuclear, Facultad de Física, Universidad de Sevilla, Spain. Before working in Sevilla, he was a Marie Curie postdoctoral fellow, a Ramón y Cajal Fellow, and a staff researcher at the University of the Basque Country. Before that, he was a Humboldt Fellow and a Max Planck postdoctoral fellow for three and a half years at the Max Planck Institute for Quantum Optics in Garching, Germany. Previously, he carried out his Ph.D. at CSIC, Madrid.

Pedro Pérez-Fernández is an associate professor (Profesor Titular de Universidad) at the Departamento de Física Aplicada III, Escuela Técnica Superior de Ingeniería, Universidad de Sevilla, Spain. He carried out his Ph.D. at the Universidad de Sevilla and he has held research stays at the Charles University in Prague, University of Notre Dame in the USA, Instituto de Estructura de la Materia at CSIC in Madrid, Spain, and Technische Universität Berlin in Germany. He is interested in theoretical nuclear physics, quantum phase transitions, algebraic models in physics and quantum simulation of nuclear models.